The Astrophysical Journal, 728:87 (12pp), 2011 February 20 doi:10.1088/0004-637X/728/2/87

THE ROLE OF ACTIVE REGION LOOP GEOMETRY. II. SYMMETRY BREAKING IN THREE-DIMENSIONAL ACTIVE REGION: WHY ARE VERTICAL KINK OSCILLATIONS OBSERVED SO RARELY?

M. Selwa[1,2,5], S. K. Solanki[3,4], and L. Ofman[1,6]
[1] Department of Physics, The Catholic University of America, 620 Michigan Avenue, NE, 200 Hannan Hall, Washington, DC 20064, USA; mselwa@mcs.st-and.ac.uk, leon.ofman@nasa.gov
[2] NASA Goddard Space Flight Center, Code 671, Greenbelt, MD 20771, USA
[3] Max-Planck-Institut für Sonnensystemforschung, Max-Planck-Str. 2, 37191 Katlenburg-Lindau, Germany; solanki@mps.mpg.de
[4] School of Space Research, Kyung Hee University, Yongin, Gyeonggi 446-701, Republic of Korea
Received 2010 October 28; accepted 2010 November 24; published 2011 January 25

ABSTRACT

We present numerical results of simulations of kink oscillations of coronal loops in an idealized active region (AR) that is initialized as a potential dipole magnetic configuration with gravitationally stratified density. We consider loops, with density higher than the surrounding plasma, embedded into the dipolar AR. We study the excitation of kink oscillations of such loops by velocity pulses at different positions, of a given duration and amplitude. The position of the pulse varies in the parametric studies. For a central (symmetric) loop within the AR, we find that the amplitude of vertical kink oscillations is significantly amplified in comparison to horizontal kink oscillations for exciters located centrally (symmetrically) below the loop. For pulses initiated further from such a symmetric loop a combination of vertical and horizontal oscillations is excited. The scenario changes significantly when we study an inclined loop (non-symmetric within a dipole field). In this case, we do not see vertical kink oscillations of any significant amplitude being excited, while horizontal ones can be easily detected. These results indicate that the reason why vertical kink oscillations are observed so rarely is that their excitation requires a set of conditions to occur simultaneously: the exciting pulse must be located roughly below the loop apex and the loop itself must be located symmetrically within the group of loops. The new findings of the present study show the importance of not only the position of the pulse, but mainly of the location of the loop within the set of field lines having the same magnetic connectivity. We find that the slow propagating wave is excited in all the studied loops and its excitation does not depend either on the geometry of the loop or the pulse. We discuss *TRACE* observations of coronal loop oscillations in view of our findings and find that our results can be used for identifying the polarization of the kink mode based on the location of the loop within the set of field lines of the same connectivity and the position of the flare.

Key words: magnetohydrodynamics (MHD) – Sun: corona – Sun: oscillations

Online-only material: color figures

1. INTRODUCTION

Solar missions such as the *Solar and Heliospheric Observatory* (*SOHO*) and the *Transition Region and Coronal Explorer* (*TRACE*) resulted in the detection of various oscillation modes in solar coronal loops. Among them we can distinguish propagating (Berghmans & Clette 1999; Robbrecht et al. 1999; De Moortel et al. 2002) and standing (Kliem et al. 2002; Wang et al. 2002) slow magnetosonic waves as well as fast kink magnetosonic waves: (Nakariakov et al. 1999; Aschwanden et al. 1999, 2002; Schrijver et al. 2002; Wang & Solanki 2004) and short-period fast sausage waves (Nakariakov et al. 2003; Aschwanden et al. 2004).

Fast kink waves consist of two kinds of oscillations: horizontal (Nakariakov et al. 1999; Aschwanden et al. 1999, 2002; Schrijver et al. 2002; Verwichte et al. 2004) and vertical (Wang & Solanki 2004) ones. Both kinds lead to an asymmetric displacement of the loop, with the difference, however, that vertical oscillations are planar oscillations while horizontal oscillations are fully three-dimensional oscillations. These oscillations affect loop properties in different ways: vertical oscillations can change the loop length and as such are compressible, while the loop length remains fixed for horizontal oscillations. Other properties, such as period and damping time, do not vary significantly between these types or polarizations of kink-mode oscillations. An intriguing and not yet explained result is that vertical oscillations are detected less often than their horizontal counterparts. Horizontally polarized oscillations have been extensively studied by, e.g., Nakariakov et al. (1999), Aschwanden et al. (1999, 2002), Schrijver et al. (2002), Verwichte et al. (2004), versus one example of the vertically polarized mode described by Wang & Solanki (2004). Recently, Wang et al. (2008) re-examined 14 of the oscillations described by Aschwanden et al. (2002) and found that two oscillations previously considered as fundamental horizontal mode oscillations are better described by the fundamental vertical mode (but possibly combined with the fundamental horizontal mode), while another was a combination of the fundamental vertical and horizontal modes. In three other cases, it was not possible to clearly distinguish between the fundamental mode and the second harmonic of the horizontal oscillation and in five other cases it was not possible to clearly distinguish between a fundamental horizontal mode and the second harmonic of the vertical mode. This study leads to the conclusion that combinations of different polarizations

[5] Current address: School of Mathematics and Statistics, University of St. Andrews, North Haugh, St. Andrews, Fife, KY16 9SS, UK.
[6] Visiting Associate Prof., Department of Geophysics, and Planetary Sciences, Tel Aviv University, Ramat Aviv, Tel Aviv, Israel.

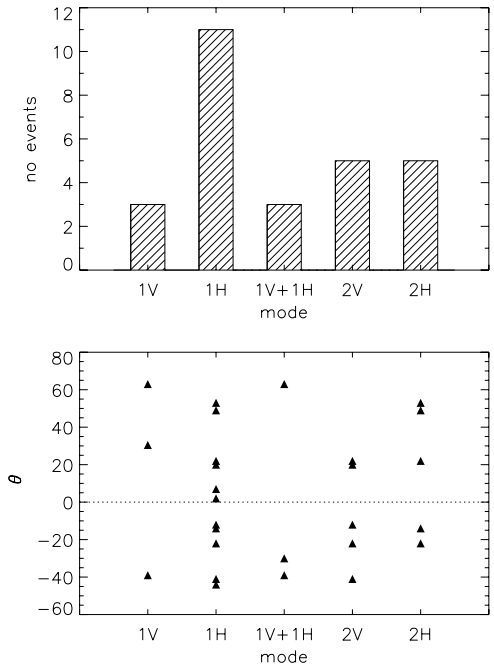

Figure 1. Top panel: histogram of kink oscillations analyzed by Wang et al. (2008) and Wang & Solanki (2004). Based on data from Wang et al. (2008; the number of displayed events is nearly doubled compared to the number analyzed by the Wang et al. 2008 data as we plot both the possible modes allowed by the data for the cases for which it is impossible to clearly identify the oscillation as a unique mode (or mode combination)) and Wang & Solanki (2004). Bottom panel: loop plane inclination angle to the vertical, θ, vs. mode of kink oscillation. Notation (1H, 1V, 2H, 2V) corresponds to the fundamental (second harmonic) of horizontal and vertical modes, respectively, while 1V+1H stands for the combination of multiple fundamental modes. The dotted line shows the position of the vertical loop in the AR.

may be common and single vertical oscillations happen less often than horizontal ones (see histogram in the top panel of Figure 1).

Theoretical studies of kink oscillation have been widely performed. Reviews of recent work on oscillation properties including effects like stratification, expansion, twist, non-circular cross-section, curvature, and collective behavior have been given by Nakariakov & Verwichte (2005) and Ruderman & Erdélyi (2009). More properties of oscillations in curved structures are provided by Van Doorsselaere et al. (2009). In particular, two polarizations of kink oscillations were studied theoretically by Van Doorsselaere et al. (2004). The authors found that quasi-mode frequencies are unchanged up to first order in the curvature by solving linearized ideal MHD equations in the zero β regime. However, the imaginary part of the frequency changes in first order, and quasi-modes are slightly more damped in realistically curved coronal loop configurations. As vertical oscillations are planar, there are several two-dimensional numerical studies of vertical oscillation properties in curved loops, e.g., Selwa et al. (2005, 2006, 2007), Brady & Arber (2005), Brady et al. (2006), Gruszecki et al. (2006), and analytical studies of vertical kink oscillations in a two-dimensional arcade, e.g., Díaz et al. (2006), Díaz (2006), who studied different harmonics, and Verwichte et al. (2006a, 2006b, 2006c), who focused on trapped and leaky modes depending on Alfvén speed profiles.

Full three-dimensional simulations allow both kink-mode polarizations to be investigated. Recently, simultaneously excited vertical and horizontal oscillations were modeled by McLaughlin & Ofman (2008). Pascoe et al. (2009) studied impulsively excited oscillations in an arcade loop. Even though the authors focused on studying the transversal mode, they found that for large values of the attack angle (the angle between the impacting velocity pulse and the loop measured at the height of the loop apex with respect to the line perpendicular to the loop in horizontal direction) the slow mode was excited, whereas for intermediate values the second harmonic of the kink mode was also excited. Selwa & Ofman (2009) studied transverse oscillations in a three-dimensional curved gravity-free loop and the slow standing mode in a curved dipolar stratified loop. Selwa & Ofman (2010) discussed the possible excitation mechanism of kink oscillations by comparing the time signatures from simulations with observed ones. These authors found that the particular curved topology of active region (AR) loops strongly affects the dynamics of loop oscillations, and needs to be taken into account in coronal seismology. For more examples of three-dimensional MHD studies of loops please refer to the recent review by Ofman (2009).

Selwa et al. (2010, hereafter Paper I) presented the effect of the AR loop geometry on coronal seismology. They showed that the loop geometry determines the effective length of the oscillating loop and hence the period of oscillation. Neglecting this can lead to significant errors in the coronal magnetic field deduced from the oscillations.

In this paper, we focus mainly on simulations of fast kink oscillations excited by a flare, in particular on finding an explanation why most of the observed oscillations have horizontal, not vertical polarization. Other mechanisms that were suggested for excitation of horizontally polarized kink mode are vortex shedding related to coronal mass ejections (CMEs; Nakariakov et al. 2009) and excitation by peculiarities of the magnetic configuration (Schrijver & Brown 2000). We use an AR loop model similar to that described in Paper I and vary the properties of the pulse and the loop in order to better understand the mechanisms of excitation and damping of both kinds of kink oscillations. The model of the loop described by Selwa & Ofman (2009) is extended in our present study by introducing gravitational stratification to the system and performing more parametric studies of different pulses and types of loops (in particular different locations of the loop in the model AR).

The paper is organized as follows: the numerical model is briefly described in Section 2. The numerical results are presented in Section 3. Section 4 describes the comparison of numerical simulations with observational data. This paper is concluded by a short summary of the main results in Section 5.

2. NUMERICAL MODEL

Descriptions of the code of the MHD model that we use, together with all the units and implemented boundary conditions, can be found in Paper I. A detailed description of how the loop is implemented into the system is also provided in Paper I. Here, we just mention briefly the two kinds of loop geometries studied in the present paper: *closed* geometry and *open* geometry. They are shown in the top panels of Figure 2. The *closed* geometry loop is defined as a loop which has maximum separation between its legs at the middle of the loop's height, while the *open* geometry loop has a maximum separation between its legs at the footpoints. In addition, we have also considered *inclined* loops (with both these geometries, shown in the bottom panels of Figure 2) which allow us to study non-symmetric loops within an AR. The inclination angle of the axis of the *inclined* loop shown in Figure 3 relative to the solar surface is 73°. The loop width at the apex is 1.22 L_s, where $L_s = 69.55$ Mm is the spatial normalization. The loop is sufficiently wide to be well

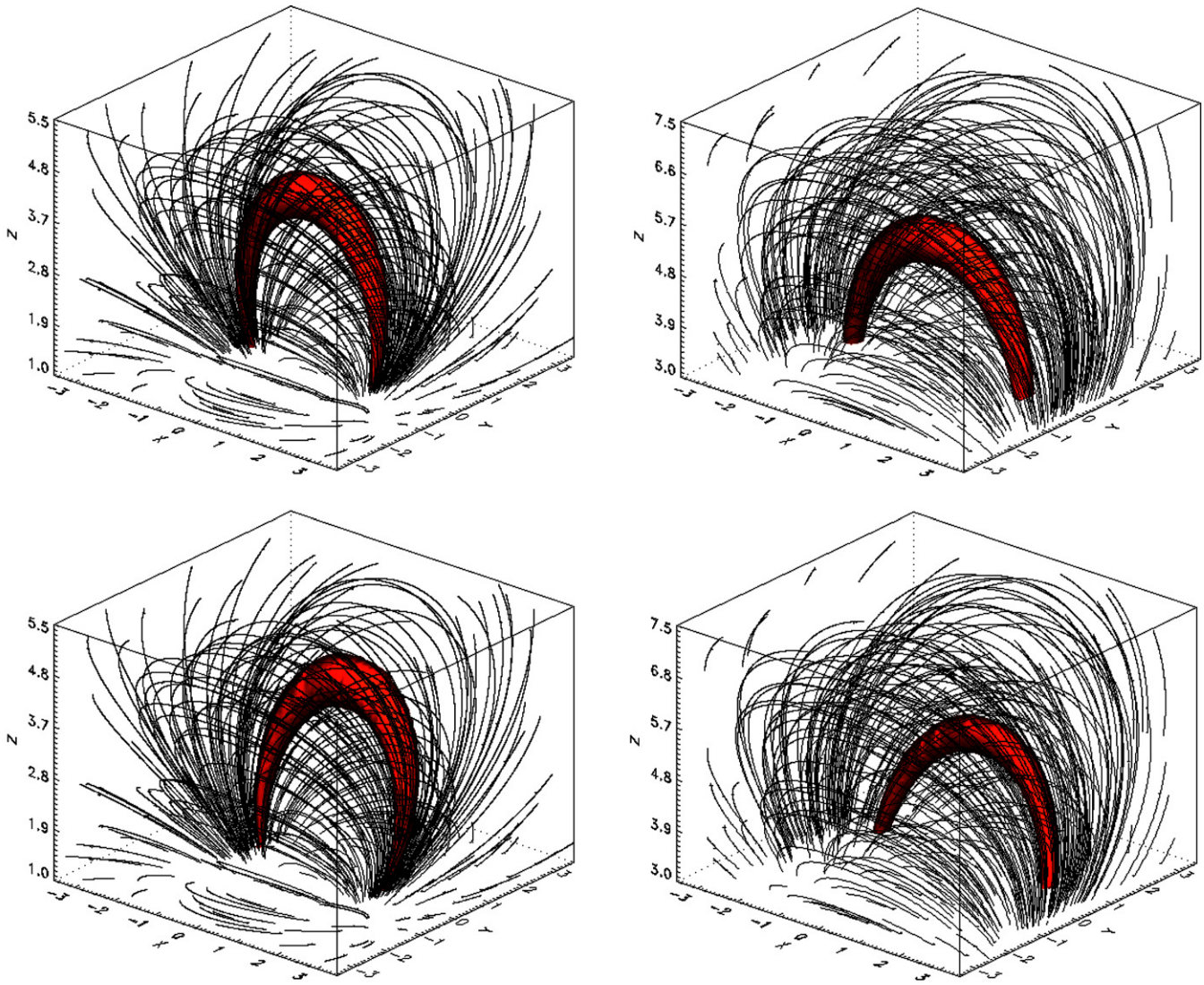

Figure 2. Initial three-dimensional magnetic field configuration of the magnetic field with the flux tube loop for the closed geometry (left panels) and open geometry (right panels) loops. Top panels show the central AR loop (adapted from Paper I) while bottom panels show the corresponding inclined loops. We present the field lines together with the isosurface of density. Note that gravitational stratification is neglected in both cases in order to display the loop more clearly (but the oscillations are computed in the presence of gravitational stratification). Spatial coordinates are measured in units of L_s.

(A color version of this figure is available in the online journal.)

resolved in our model. The width of the loop ranges between 0.04 of the loop's length near footpoints and 0.16 of the loop's length near the loop top represents a bundle of threads that are seen to oscillate in phase (Aschwanden et al. 2002).

2.1. The Perturbation

In order to excite kink oscillations we perturb the loop in the following ways. First, a velocity pulse is launched at the $(x-z)$-boundary plane along $y_{\min}$, which models the impact of an initially horizontally propagating fast magnetoacoustic wave on our AR (e.g., Selwa & Ofman 2009, 2010):

$$V_y = A_V V_{A0} \exp\left[-\left(\frac{x-x_0}{w}\right)^2\right] \exp\left[-\left(\frac{z-z_0}{w}\right)^2\right] \times \exp\left[-\left(\frac{2t-\left(t_1+\frac{t_2-t_1}{2}\right)}{t_2-t_1}\right)^8\right]. \quad (1)$$

Here, $A_V = 0.1$ is the amplitude of the pulse relative to V_{A0}, which is the maximum Alfvén speed at the bottom of the simulation region, $t_1 = 2.5\tau_A$, $t_2 = 7.5\tau_A$ $x_0 = 0$, $z_0 = z_{\max}/2$, and $w = 1.0$.

Another type of perturbation considered here models an impulsive event (flare) centered below (or somewhat to the side of) the loop (velocity pulse launched at the bottom boundary, used by, e.g., Selwa & Ofman 2009):

$$V_z = A_V V_{A0} \exp\left[-\left(\frac{x-x_0}{w}\right)^2\right] \exp\left[-\left(\frac{y-y_0}{w}\right)^2\right] \times \exp\left[-\left(\frac{2t-\left(t_1+\frac{t_2-t_1}{2}\right)}{t_2-t_1}\right)^8\right], \quad (2)$$

where $A_V = 0.1$, t_1, t_2, and w have the same values as in Equation (1). We vary the position of the pulse given by Equation (2) in parametric studies: $x_0 = 0$, $y_0 = 0$ (referred

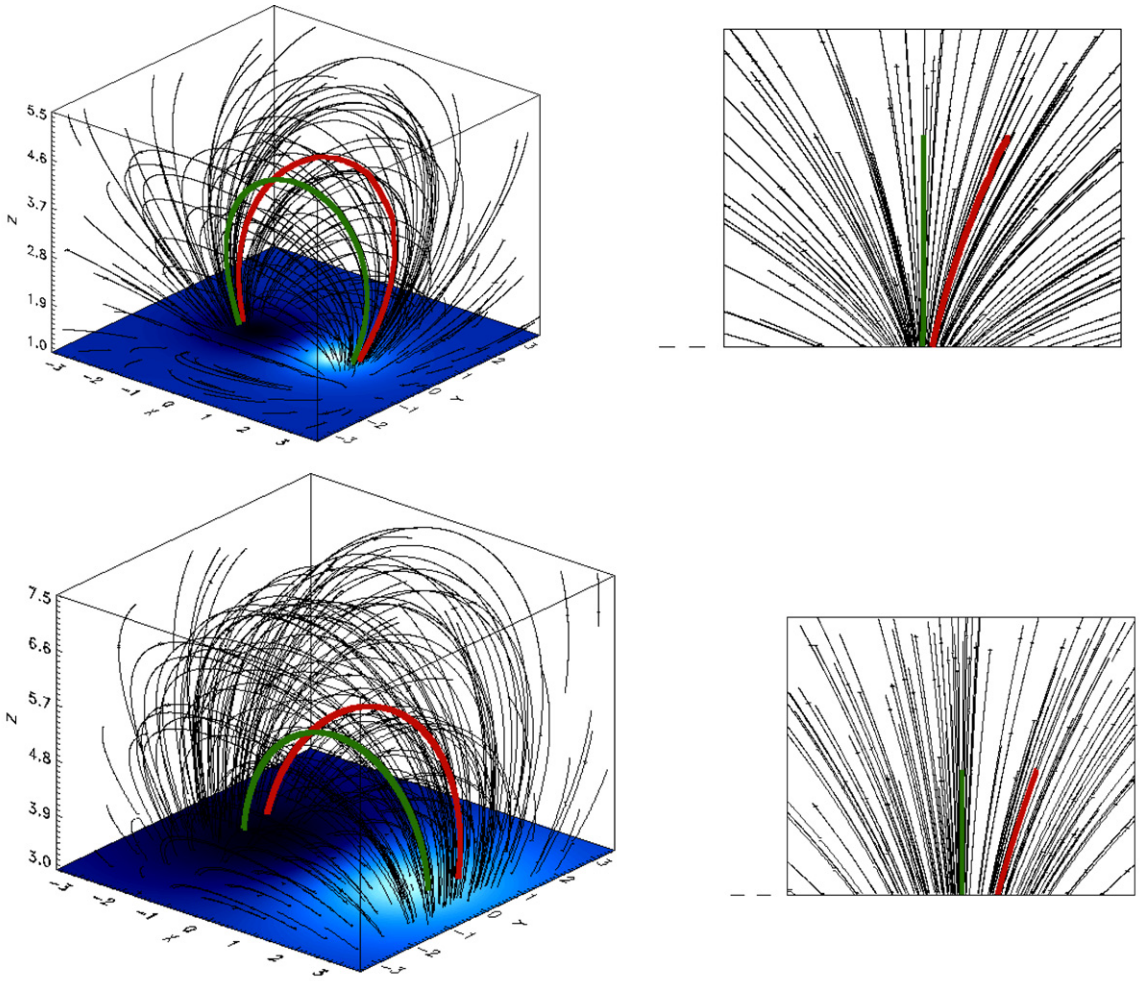

Figure 3. Initial three-dimensional magnetic field configuration of the magnetic field in the closed (top panels) and open geometry (bottom panels) with the axes of the central (thick green line) and inclined (thick red line) AR loop seen from two different angles. Spatial coordinates are measured in units of L_s.
(A color version of this figure is available in the online journal.)

to as pulse A), $x_0 = 0$, $y_0 = 1$ (B), $x_0 = -0.75$, $y_0 = 0$ (C), $x_0 = -0.75$, $y_0 = 1$ (D), $x_0 = 0$, $y_0 = 2$ (E), $x_0 = -1.3$, $y_0 = 1$ (F), $x_0 = -2.2$, $y_0 = 0$ (G). The y (z)-plane pulse perturbations, with the loop profile (loop footpoints) overplotted, are shown in Figure 4.

3. NUMERICAL RESULTS

3.1. Central (Symmetric) Loop within AR

We start our studies with the central loops shown in the top panels of Figure 2. We extend the study presented in Selwa & Ofman (2009) and in Paper I by investigating the influence of the position of the pulse on the relative amplitude of the horizontal and vertical mode. We vary the position of the pulse as shown in the bottom panel of Figure 4. The position of the pulse does not change the difference images of the oscillations (not shown; such images have been presented and discussed in Paper I for a pulse in the vertical component of velocity, V_z, located exactly below the loop (bottom panel of Figure 4, Equation (2), case A)). However, the ratio of the maximum amplitude of the vertical ($V_v = V_z$) component to the horizontal ($V_h = V_y$) component of velocity, V_z/V_y, at the loop's apex varies with the position of the pulse. Table 1 shows the ratios for both loop geometries and all types of excitation.

Typical time signatures of V_z (solid line) and V_y (dashed line) excited by pulse A from the bottom panel of Figure 4 (Equation (2)) are shown in the top panels of Figure 5. The pulse reaches the detection point at $t \simeq 15$ and excites mainly vertical (V_z) oscillations. The small amplitude motions before $t = 15$ are due to the adjustment phase (Ofman 2007; McLaughlin & Ofman 2008; Selwa & Ofman 2009, 2010) as we do not start simulations from a strict analytical equilibrium. Due to the very small amplitude of the horizontal oscillation in comparison to the vertical one this polarization is very unlikely to be observed (see the dotted line in Figures 5(a) and (b)), while the vertical oscillation is expected to show a clear displacement in observations (note the difference in scales in Figures 5(a) and (b)). Note that some time signatures of the vertical (V_z) component of velocity show the permanent offset of the loop's apex (clearly shown in Figure 5(c)). This offset has been seen in earlier studies (Selwa et al. 2005, 2006, 2007) and is produced by the larger amplitudes of the oscillation at the expanding compared to the shrinking phases (due to damping).

Note that for all the pulses centered along the $y_0 = 0$ line (i.e., below the loop's apex, which corresponds to cases A, C, G described by Equation (2) and plotted in the bottom panel of Figure 4) the ratio of the vertical to horizontal velocity component amplitudes is close to ~50, so that only the vertical

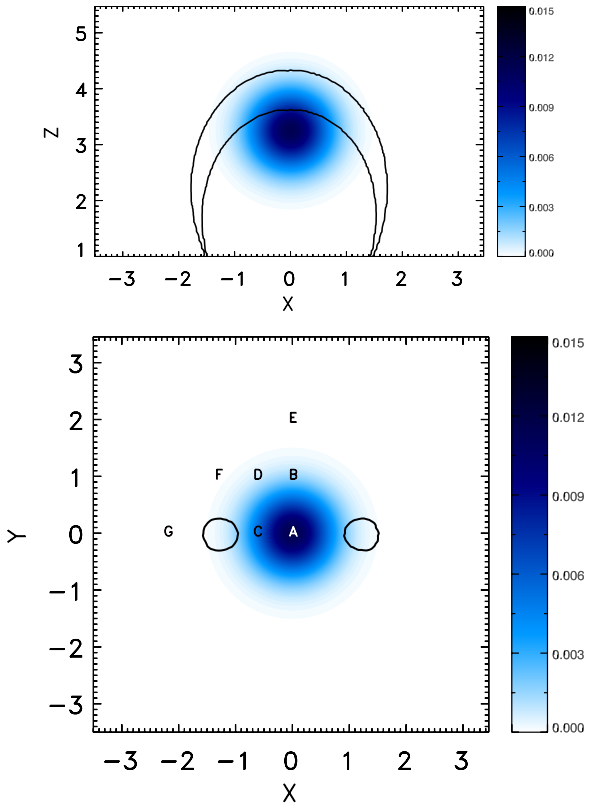

Figure 4. Spatial profiles of the pulses launched in the y-component of velocity (top panel, $x-z$ plane, replotted after Selwa & Ofman 2009) and in the z-component of velocity (bottom panel, $x-y$ plane; color scales). Black contours display the initial position of the loop (which lies in a different plane from the pulse in the top panel). Letters in the bottom panel mark the positions of the centers of the various pulses. Spatial coordinates are given in units of L_s.

(A color version of this figure is available in the online journal.)

kink mode is excited when the pulse lies anywhere along the line connecting the footpoints of a centrally located loop within a dipolar AR. However, a pulse located further from the line connecting the loop footpoints (cases B, D, F in the bottom panel of Figure 4; Equation (2)) produces a significantly stronger horizontal oscillation, which could possibly even be detected with a sensitive instrument as its amplitude reaches 10%–20% of the vertical oscillation's amplitude. For pulses located relatively far from the loop (case E in the bottom panel of Figure 4; Equation (2)) the amplitude of horizontal oscillations is a factor of <3 lower than the vertical amplitude and both oscillations should be detected simultaneously as a combination of modes (see Table 1 and Figures 5(c) and (d)).

A pulse originating very far from the loop was modeled as a pulse from the side boundary (top panel of Figure 4; Equation (1)). The combination of horizontal and vertical oscillations is seen in difference images of *open* geometry loops shown in Figure 6, although the simultaneous presence of the vertical oscillation makes the image less clear. The damping mechanism of kink oscillations has been discussed in Paper I.

3.2. Non-symmetric (Inclined) Loop within AR

Most of the observed kink oscillations are horizontal oscillations (Nakariakov et al. 1999; Aschwanden et al. 1999; Schrijver et al. 2002; Wang et al. 2008). We showed in Section 3.1 that in a loop located symmetrically within the AR vertical oscillations are always excited for a rather wide set of locations of the exciter (pure ones if the pulse is located below the loop and as a combination of vertical and horizontal modes in the case of distant pulses). This seeming contradiction with observations may be due to the rather special location of the loop considered so far.

Table 1
Ratio of Vertical ($V_v = V_z$) to Horizontal ($V_h = V_y$) Velocity Components[a] at the Loop's Apex for Different Perturbations and Geometries of a Vertical (Symmetrically Located) Loop

Loop	Perturbation	V_v/V_h	Loop	Perturbation	V_v/V_h
c	I	∼50	*o*	I	∼50
c	A	∼50	*o*	A	∼50
c	B	∼10	*o*	B	∼7.5
c	C	∼50	*o*	C	∼50
c	D	∼7.5	*o*	D	∼7.5
c	E	∼3	*o*	E	∼2
c	F	∼10	*o*	F	∼5
c	G	∼50	*o*	G	∼50
c	Y	∼1.5	*o*	Y	∼2

Notes. Perturbations A–G correspond to the different locations of the bottom boundary pulse (bottom panel of Figure 4, Equation (2)), I denotes initial perturbation (initial perturbation consists of three-dimensional Gaussian structure below the loop, and is not imposed as a boundary condition but as an initial condition. Boundary pulse is imposed in a two-dimensional plane ($x-y$ in the case of perturbations A–G or $x-z$ for perturbation Y), and is a time-dependent perturbation.) (Figure 2, Equation (14) from Paper I) and Y is the side boundary pulse (top panel of Figure 4, Equation (1)). Loop geometries are marked as *c* for *closed* and *o* for *open* geometry loops, respectively.

[a] Determined for the first two peaks in time signatures.

In order to examine how the location of the loop affects the excitation of a particular wavemode we concentrate now on an *inclined* loop, i.e., one not located at the very center of the AR. The axes of the considered *inclined* loops having *closed* and *open* geometry are marked in Figure 3 by red thick lines. The central loops are highlighted by the thick green lines.

We perturb the *inclined* loops with two kinds of pulses: one from below (case A from the bottom panel of Figure 4, Equation (2)) and one from the side (the top panel of Figure 4, Equation (1)). The simulations presented in Section 3.1 suggest that these are the two most extreme pulses as far as exciting horizontal versus vertical modes is concerned. We will continue to use the name "vertical" to describe the planar ("breathing" type) mode and "horizontal" for a true three-dimensional transverse mode also in the case of an *inclined* loop. However, now the "vertical" direction refers to the direction of the axis of the loop. The corresponding time signatures of vertical (solid lines) and horizontal (dashed lines) velocity components are shown in Figure 7. We see that for both kinds of excitation and both kinds of loop geometry the horizontal mode is dominant and the vertical component is partly associated with loop adjustment to the equilibrium (i.e., even when perturbed from below the loop first shrinks then expands and does not lead to an offset). This suggests that non-symmetric loops within the AR display mainly the horizontal kink-mode oscillation. Therefore, in most of the cases no vertical oscillation can be detected.

In order to verify how sensitive this result is to the inclination angle we consider additionally two more loops of *open* geometry (indicated in the top panel of Figure 8 by the blue and light green lines): highly and slightly *inclined* (with inclination angles of the loop's axis relative to the solar surface being 65° and 81°, respectively). Simulations involving these new loops confirm that irrespective of the pulse type and inclination angle the horizontal kink oscillation is mainly excited in *inclined* loops,

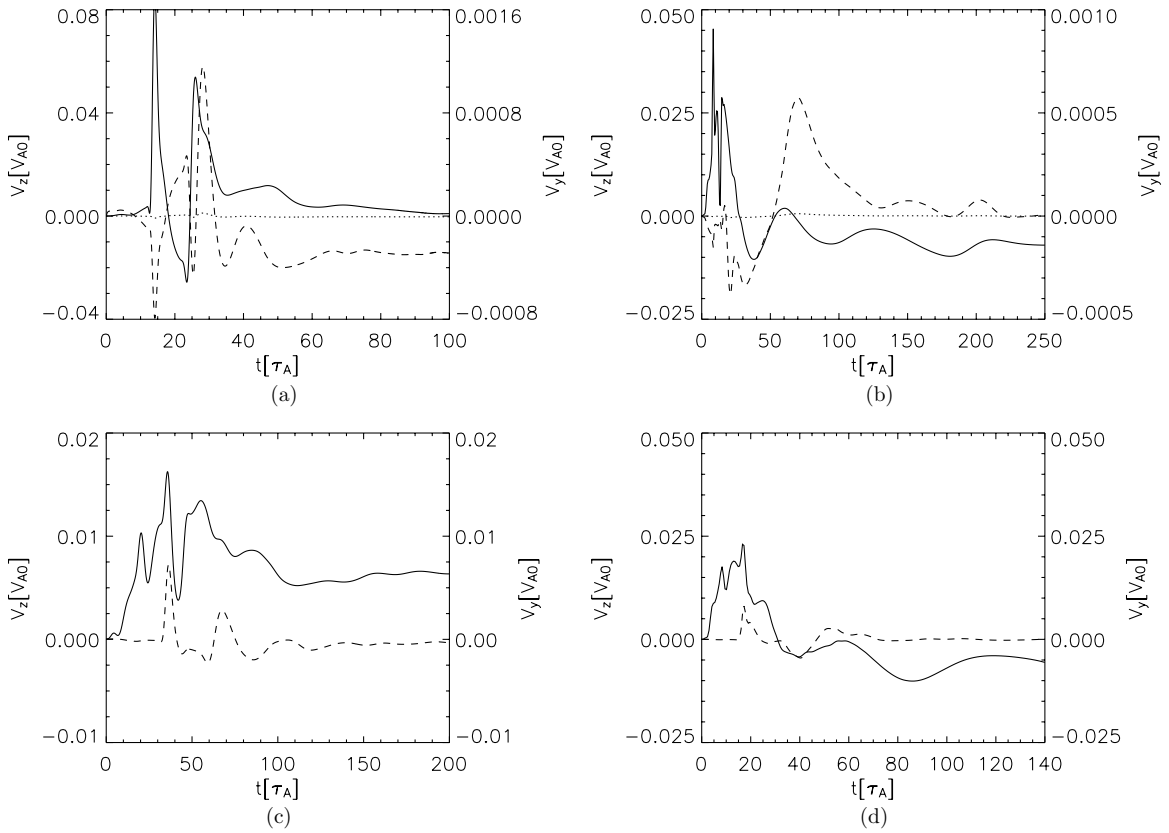

Figure 5. Time signatures of the vertical (V_z, solid line) and horizontal (V_y, dashed line) components of velocity collected at the closed (panels (a) and (c)) and open (panels (b) and (d)) geometry loop's apex perturbed by a bottom boundary pulse corresponding to the bottom panel of Figure 4, case A (panels (a) and (b)), and by a side boundary pulse corresponding to the top panel of Figure 4 (panels (c) and (d)). The dotted line in the top panels represents the horizontal velocity component plotted on the same scale as the vertical velocity component.

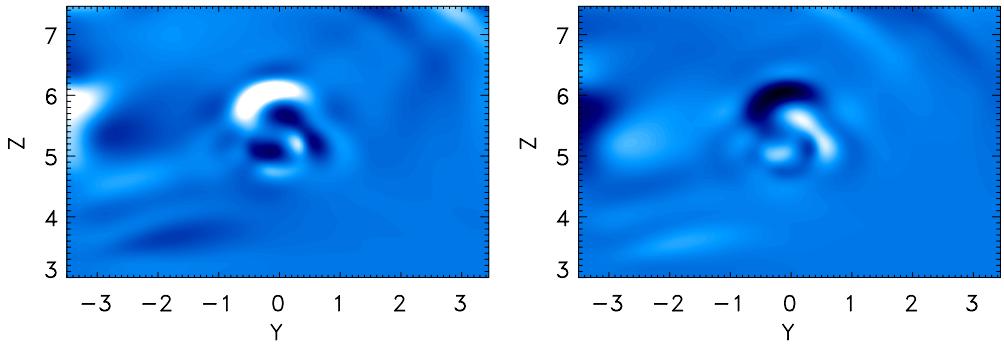

Figure 6. Difference images in the y–z plane (at $x = 0$) of mass density of the *open* geometry loop between the initial state and the first maximum in time signature (left panel) and between the first maximum and the first minimum (right panel), respectively. The perturbation is launched as a $y_{\min}$ boundary pulse (corresponding to the top panel of Figure 4). Light (dark) blue areas correspond to an increase (decrease) in density. Spatial coordinates are given in units of L_s. Note that the oscillation displayed here is not a purely horizontally polarized kink mode, but a combination of horizontal and vertical polarizations, so that difference images also show signatures of vertical motions.

(A color version of this figure is available in the online journal.)

i.e., loops located non-centrally in the modeled field (middle and bottom panels of Figure 8).

The simulations clearly show a difference between the central, vertical loop, and other, more *inclined* loops regarding their preference to oscillate more horizontally or vertically. It could be an intrinsic property of the loops, e.g., of the modeled magnetic structure, or it may have to do with the fact how the velocity pulse hitting the considered is directed. Recall that the ratio of vertical to horizontal oscillation amplitude of the central loop depends strongly on the location of the pulse (Section 3.1). Consequently, let us consider now the velocity perturbation. A perturbation directed exactly from the bottom (Figures 9(a) and (b)) leads to an exactly vertical motion when it reaches the apex of the central loop considered here. In the case of central loop, the dominant component all along the loop is vertical. This may arise from the symmetric variation of the fast magnetosonic speed as a function of distance from the loop on both sides of the central loop, affecting transverse wave leakage. After the pulse deposits a fraction of the energy in the loop, the oscillation's phase speed and leakage is determined by the local AR magnetic and density structure (e.g., Ofman & Thompson 2002).

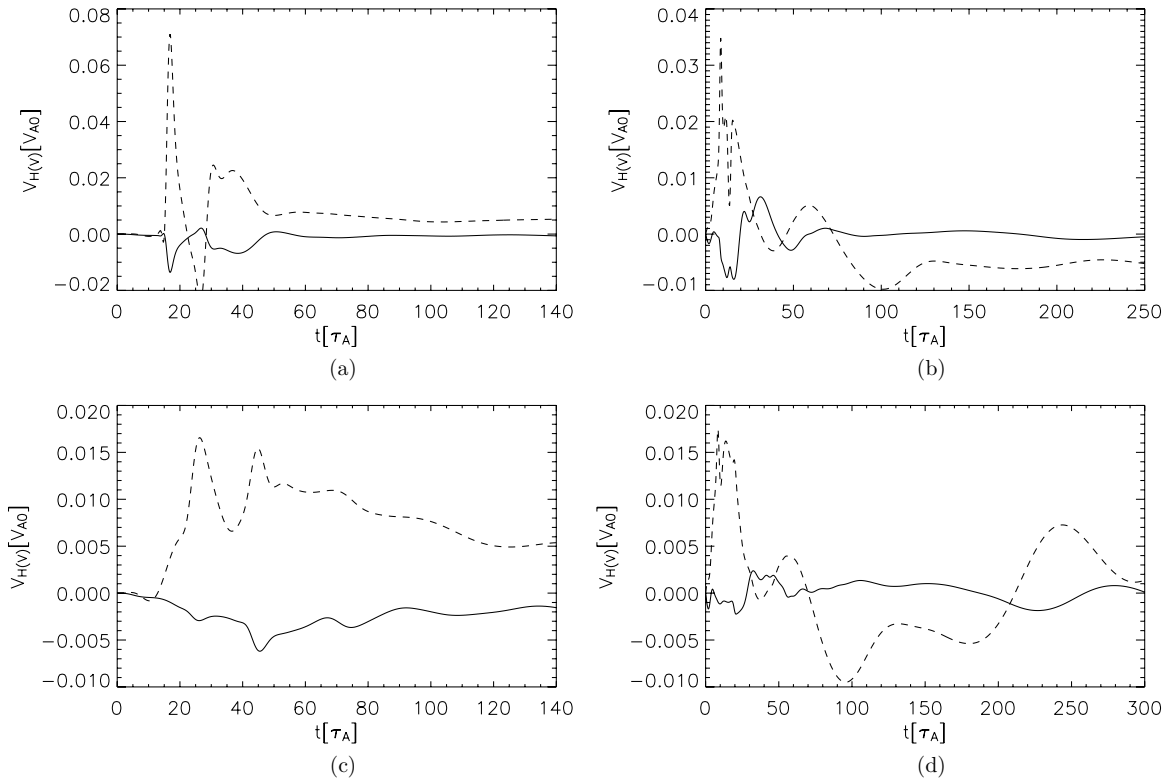

Figure 7. Time signatures of the vertical (V_v, solid line) and horizontal (V_h, dashed line) components of velocity collected at the apex of inclined loops having closed (panels (a) and (c)) and open (panels (b) and (d)) geometry perturbed by a bottom boundary pulse corresponding to the bottom panel of Figure 4, case A (panels (a) and (b)), and by a side boundary pulse corresponding to the top panel of Figure 4 (panels (c) and (d)).

When the pulse is launched from the side boundary (Figures 9(c), (d), and (e)) the central AR loop is perturbed both in the horizontal and the vertical direction (Figure 9(e)), so that the loop oscillates in a combination of vertical and horizontal kink modes. The reason for this combined excitation lies in the propagation of the pulse launched at the side, which in turn depends on the fast-mode speed. For an isothermal atmosphere this varies according to the Alfvén speed, which decreases with height. This causes the velocity front to get a component pointing upward, producing a vertical component of the exciting velocity.

Let us now consider *inclined* loops, starting with the pulse originating from below. As the fast wave corresponding to the pulse moves with different speed along and across the field lines, we expect that the angle between vertical (V_z) and horizontal (V_y) components of velocity, α_V, will not follow the inclination angle of the detection point, θ, which corresponds roughly to the inclination of the loop axis to the solar surface normal. Figure 10 shows both the inclination angle of detection points, i.e., the points where we sample the velocity and magnetic field (dotted lines), and the angle between velocity components (solid lines) versus position along the y-axis. Considered first is the set of detection points lying along the velocity front (marked with the corresponding "×" signs). From the inclination angle distribution along the wave front (points marked with the corresponding "×" signs in panel (c) of Figure 10) one could naively conclude that loops of any inclination should perform mainly vertical oscillations at least for a pulse coming from below. However, the simulations clearly show that both in the case of slightly ($y_{\rm apex} = 0.75L_s$) and highly ($y_{\rm apex} = 2.25L_s$) *inclined* loops the ratio of vertical to horizontal component of the excited oscillatory velocity at the apex is of the order of 0.1, so that in both cases only horizontal oscillations are observed. The discrepancy between the predicted and observed in simulation modes argues that the excitation of almost purely horizontal oscillations in *inclined* loops is not due to a chance cross-alignment of pulse velocity and loop axis. The same is also true for the pulse from the side. Because the *inclined* loops studied here are pointing in the positive y-direction, i.e., away from the pulse, there is always a significant component of the pulse velocity aligned with the loop axis also in this case. A more promising analysis would consider both the (frequency and direction) spectra of the pulse, $F(\omega)$, and the response function of the loop, $R(\omega)$, to the excitation. The detected eigenmode of small amplitude (linear) oscillation can be explained by the convolution $F(\omega) \star R(\omega)$ all along the loop length. Such an analysis lies beyond the scope of the present paper. However, we note that the key point determining the polarization of kink oscillation is the magnetic structure and its response to the pulse. It is also worth considering the velocity along the points marked with green plus symbols in panel (a) of Figure 10 lying along a line parallel to the velocity front (panel (b) of Figure 10). We see that the further away from the center of the AR, the larger the difference between inclination of the detection point and velocity angles is. The velocity distribution along the line parallel to the wave front suggests that as a result of the field response the velocity starts to deviate from the vertical direction, which leads to mainly horizontal oscillations.

From the study of *inclined* loops we conclude that the location of the loop within the AR is far more important than the relative location of the exciter in determining whether a horizontal or vertical wavemode is set up. Note that in a simple dipolar AR, such as the one considered here, the central (symmetric) line happens to be also the one supporting vertical loops. However,

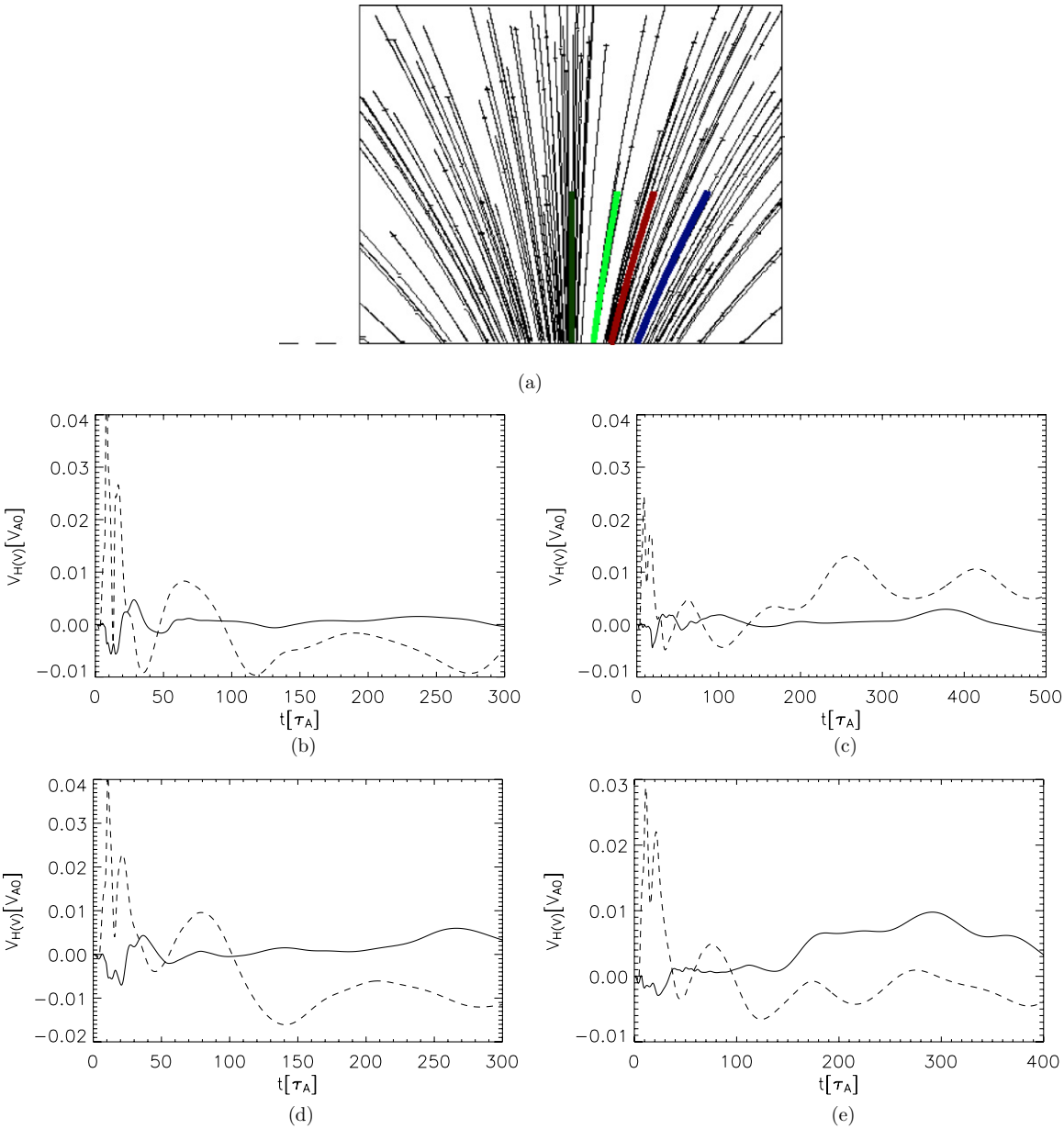

Figure 8. (a) Initial three-dimensional magnetic field configuration of the magnetic field of the open geometry with the axes of central (thick dark green line) and inclined (thick red line) AR loops. Additionally, two more loops are considered: highly inclined (thick blue line) and slightly inclined (thick light green line). Spatial coordinates are measured in units of L_s. (b)–(e) Time signatures of vertical (V_v, solid line) and horizontal (V_h, dashed line) components of velocity collected at the apex of slightly (panels (b) and (c)) and highly (panels (d) and (e)) inclined loops perturbed by a bottom boundary pulse corresponding to the bottom panel of Figure 4, case A (panels (b) and (d)), and by a side boundary pulse corresponding to the top panel of Figure 4 (panels (c) and (e)).

(A color version of this figure is available in the online journal.)

real solar ARs are generally not strictly dipolar. The topology of the magnetic field is often more complex and we do not expect that symmetric/central line in an AR to be the vertical one. Additionally, the idealized dipolar AR studied in our numerical simulations contains only two sunspots of opposite magnetic polarity. Most solar AR contain loops connecting unevenly distributed magnetic patches or even several distinct regions of opposite magnetic polarity. We speculate that in more complex cases the position of the loop within the AR field (symmetric/central or not) is probably more important than the angle of the loop relative to the vertical. By considering the inclination and location of vertically oscillating loops we can test this speculation.

3.3. Slow Wave

In all simulations we noticed a significant reduction in the density at the loop apex soon after the perturbation. In this section, we identify the cause of these long-term density variations. We plot the density at the loop's apex and its surroundings in the top panel of Figure 11. The loop is perturbed by a side boundary pulse (top panel of Figure 4, Equation (1)). We see that the plasma at the apex is rarified at $t \simeq 100$–$200\ \tau_A$ compared to its initial value. However, it gets enhanced again at $t \simeq 300\ \tau_A$. These changes coincide with the change in longitudinal component of velocity (bottom panel of Figure 11). Therefore, the variation of density is caused by a

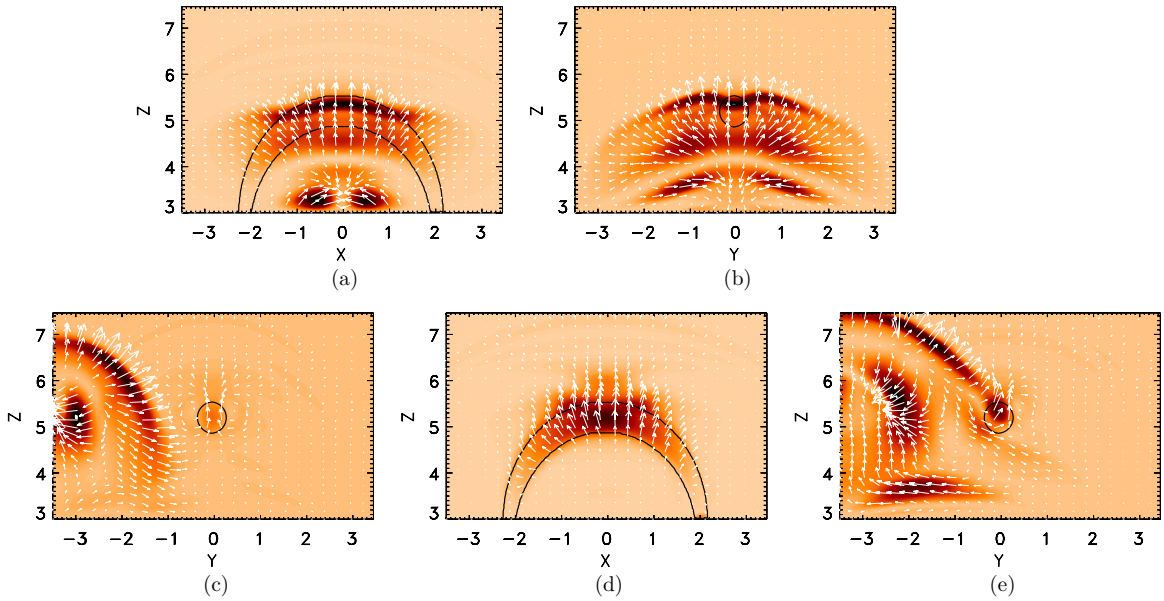

Figure 9. (a) and (b) Projected velocity of the incoming wave in the $x-z$ and $y-z$ planes at $t = 10\tau_A$ for a pulse launched at the bottom boundary (corresponding to the bottom panel of Figure 4, case A). (c)–(e) Projected velocity of the incoming wave in the $y-z$ plane at $t = 12\tau_A$ (panel (c)), $x-z$ plane at $t = 17\tau_A$ (panel (d)), and $y-z$ plane at $t = 17\tau_A$ (panel (e)), respectively, for a pulse launched at the side boundary (corresponding to the top panel of Figure 4). The velocity in the $x-z$ ($y-z$) plane is calculated using x and z (y and z) components, respectively. The arrows show the direction of the flows, and the color scale indicates the magnitude of the variable. The initial position of the central loop (of open geometry) is indicated by the black contour. Spatial coordinates are given in units of L_s.

(A color version of this figure is available in the online journal.)

slow wave and not by numerical dissipation. Similar rarifications and enhancements of plasma density at the apex due to slow wave were seen in simulations of two-dimensional arcade loop by Selwa et al. (2005, 2006, 2007). Selwa & Ofman (2009) observed excitation of a slow standing wave in an AR loop as a result of footpoint excitation, while Selwa & Ofman (2010) studied only the initial phase showing rarification of plasma density at the apex.

Verwichte et al. (2006c) presented detailed theoretical analysis of the density perturbation associated with vertically polarized kink oscillations. The authors suggested that in non-zero β plasma kink oscillations can excite nonlinearly slow oscillations and that both waves can have comparable amplitudes. However, due to timescale difference it should be easy to distinguish these modes. The excitation of a slow wave in a three-dimensional arcade loop was studied by Pascoe et al. (2009). These authors found that the slow wave was excited only for a large attack angle. In contrast, in our simulations a propagating slow wave is excited in the loop even if the attack angle is small (perturbation located exactly in front of the loop's apex, attack angle = 0). The difference in our results might be caused by the fact that our dipolar AR consists of loops for which the inclination angle varies, while in the simpler arcade considered by Pascoe et al. (2009) the loop system consists of a set of identical loops. Therefore, in a dipolar AR a pulse launched in the horizontal component of velocity reaches a loop in the interior of the AR in the form of a pulse that is a combination of different components (due to reflection and refraction) of velocity and will be capable of exciting both kink and slow waves. The comparison of our results with those of Pascoe et al. (2009) highlights the importance of the geometry of the whole AR and not just of an individual loop in determining the excitation of the oscillation modes. In most real solar ARs, we see variations in loop length and inclination. Therefore, slow waves will generally be excited, similar to our dipolar AR model result. Consequently, we expect slow-mode waves to be rather easily excited in ARs. This agrees with the large number of slow-mode oscillations found by SUMER (Wang et al. 2003) which seem to be excited by brightenings that do not count as proper flares (Wang et al. 2005, 2007). This is in contrast to the so far discovered kink-mode oscillations.

4. COMPARISON WITH OBSERVATIONS

We apply our findings to some observed loop oscillations. The idealized dipolar AR studied in our numerical simulations might be considered as a model of part of a realistic AR containing two big regions of opposite magnetic polarity and the loops connecting them. In our comparison to observations, we will focus on two specific sunspots in ARs and loops located in regions of concentrated magnetic flux rather than consider the whole AR with all minor spots and complex topology of field lines connecting several magnetic poles.

4.1. Case of the TRACE Loop in the 171 Å Channel on 2001 May 15 2:57 UT—Vertical Oscillation

We consider the loop observed by Aschwanden et al. (2002, their case 16a) and re-examined by Wang et al. (2008). Selwa & Ofman (2010) used the time signatures of this event to compare with the time signature of the oscillation excited by internal and external pulse and found out that only external excitation can reproduce observed time signatures of oscillations. Here, we focus on the magnetic topology of the AR, trying to determine if results of our studies can be applied to study observational cases and to test the speculation at the end of Section 3.2. The magnetic structure of the AR and its loops are shown in Figure 12. The oscillation of the loop presented in panel (c) of Figure 12 was first classified as a transversal one by Aschwanden et al. (2002) without distinguishing between the polarizations. Later, Wang

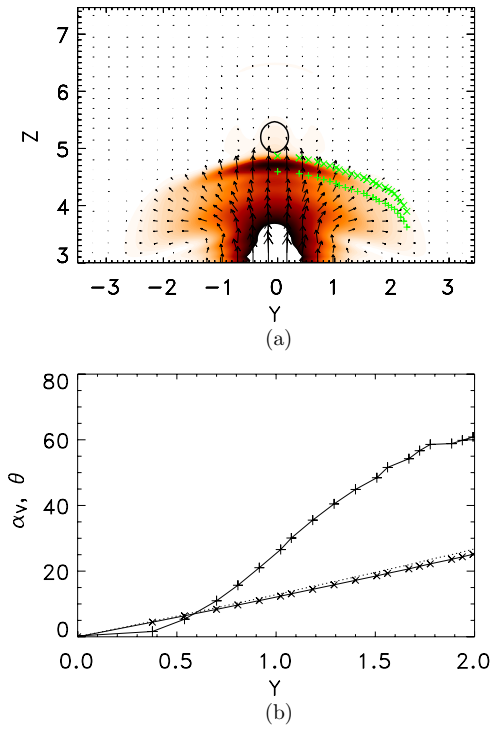

Figure 10. (a) Projected velocity of the incoming wave in the $x-z$ plane at $t = 6.5\tau_A$ for a pulse launched at the bottom boundary (corresponding to the bottom panel of Figure 4, case A). The velocity in the $x-z$ plane is calculated using x and z components only. The arrows show the direction of the flow and the color scale indicates the magnitude of the variable. The initial position of the central loop (of open geometry) is indicated by the black contour. The green "×"symbols show the position of the wave front while green "+" symbols indicate detection points inside the incoming wave, but parallel to the wave front. (b) Inclination angle of detection point, θ (dotted lines), and the angle between vertical and horizontal component of velocity, α_V (solid lines) vs. position along y-axis. Detection points are corresponding to the positions marked with "×" and "+" signs in panel (a). Spatial coordinates are given in units of L_s.

(A color version of this figure is available in the online journal.)

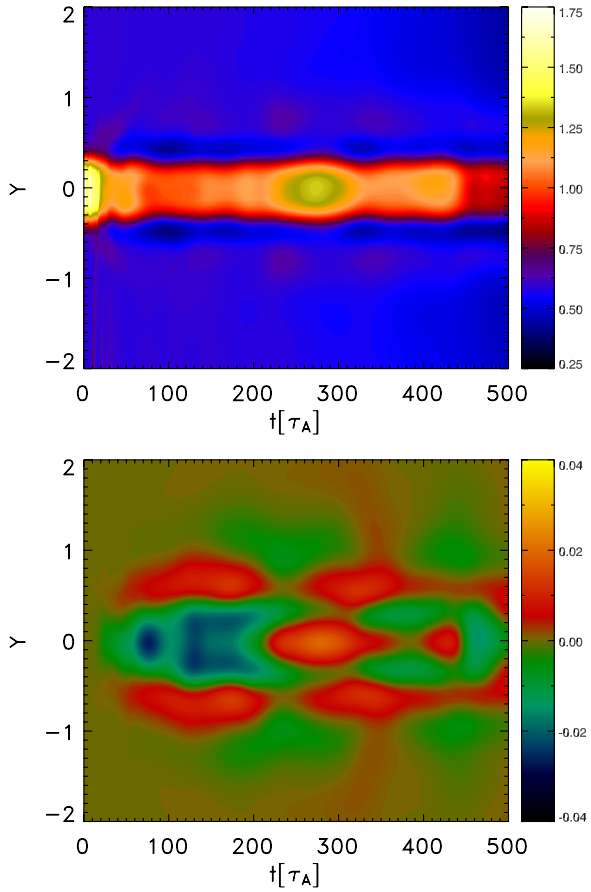

Figure 11. Time signatures (color contours, units of ϱ_0 and V_{A0}, respectively) of mass density (top panel) and longitudinal component of velocity (V_x, bottom panel) collected at the apex of the open geometry loop and its surroundings (along $x = 0$, $z = 5.25$ line). The loop was perturbed by a side boundary pulse corresponding to the top panel of Figure 4. Spatial coordinates are given in units of L_s.

(A color version of this figure is available in the online journal.)

et al. (2008) showed that the loop oscillates in the fundamental vertical mode. The loop is situated on the disk and belongs to the magnetic field lines that connect two regions of opposite magnetic polarity (panels (a) and (c) of Figure 12). According to Wang et al. (2008), the axis of this loop is inclined by 39° to the vertical. However, following our speculation, the inclination angle that matters in our study refers to the inclination within the loops located in regions of concentrated magnetic flux. From the movie presented by Schrijver et al. (2002) we clearly see that the loop is disturbed from below. As its oscillation is classified as a vertical mode, besides being perturbed from below, the loop should also be central (symmetric) within the set of field lines connecting two spots. The first of these conditions is well identified by the observations. The second condition for vertical loop oscillations is seemingly not fulfilled, however, due to the large inclination to the vertical. A significant inclination of a vertically oscillating loop is not unusual, as can be seen by considering the bottom panel of Figure 1 (based on data from Wang et al. 2008 and Wang & Solanki 2004).

Clearly, the vertical mode is excited not just in vertical loops. The discrepancy to our simulations may result from the fact that in our simulations the vertical loop happens to be also the central one, i.e., the one with a symmetric distribution of field lines on both sides. Hence, the discrepancy indicates that the factor determining the excitation of vertical modes in a loop is not the vertical orientation of the loop, but rather the symmetric (central) position of the loop within the dipolar set of field lines. As most of the AR is not strictly dipolar we decided to consider smaller scale fields connecting two well-localized regions of opposite polarity and verify the position of the loop among these field lines.

To determine if the loop from event 16a described by Aschwanden et al. (2002) and reanalyzed by Wang et al. (2008) as oscillating in vertical mode is central within the set of field lines it is embedded in, we compute a potential extrapolation of the magnetic field from a corresponding magnetogram (panels (d), (e), and (f) of Figure 12). The photospheric magnetogram extrapolated to the height of ∼3000 km, which corresponds to the lower coronal boundary, is shown in panel (b). Note that at this height the magnetogram appears smoother than in the photosphere (panel (a)), due to the rapid decay of high-order multipoles with height in the extrapolated magnetic field. The potential extrapolation is used to calculate the initial magnetic field throughout the computational domain on the basis of the Green's function approach (Cuperman et al. 1990). A number of field lines of the AR's magnetic field are shown in panels (d)–(f) of Figure 12 which compare favorably with the global structure of the AR observed with *TRACE* as seen by comparing panels (c) and (d). In the latter panel, the three-dimensional computational domain was rotated to match the line of sight

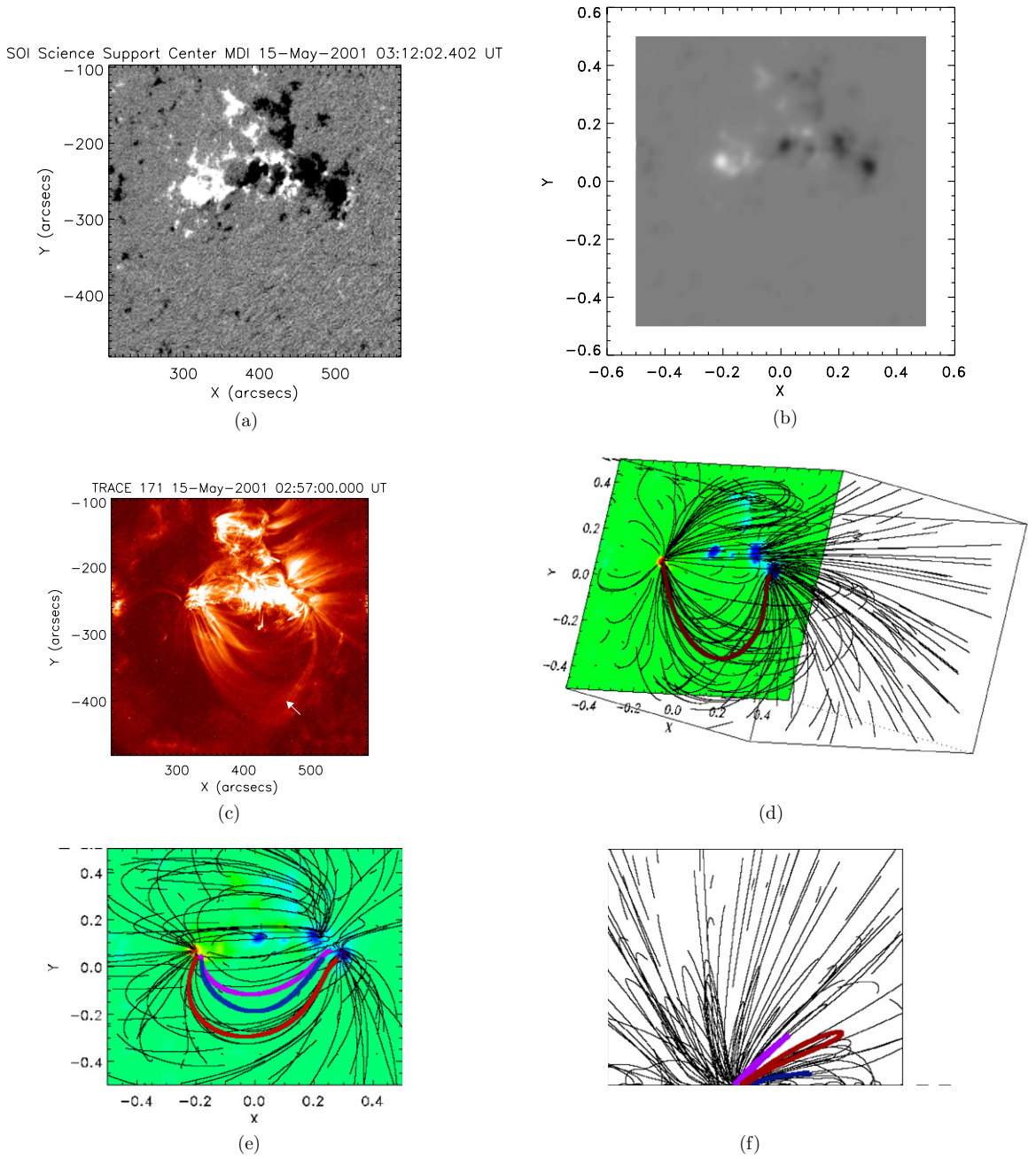

Figure 12. (a) and (b) AR loop oscillation event of 2001 May 15 2:57 UT. MDI magnetograms at 3:12 UT: magnetogram of NOAA9455 AR (panel (a)), potential extrapolation of the magnetic field from the magnetogram to the height of ∼3000 km (panel (b)). (c)–(f) *TRACE* image of the AR in the 171 Å channel (panel (c)). The arrow indicates the loop that is oscillating in fundamental vertical kink mode. The oscillation was described by Aschwanden et al. (2002), case 16a, and reanalyzed by Wang et al. (2008). Panels (d)–(f) show three viewing angles of the potential field extrapolation of the magnetogram shown in panel (a) with the oscillating loop highlighted by the thick red line. The viewing angle in panel (d) was set to approximately the line of sight of the AR on the Sun (compare to panel (c)). The field of view is marked in normalized units. In panel (e), the projection onto the solar surface is displayed while in panel (f) the projection onto the y–z plane is plotted. The purple and blue lines in panels (e) and (f) show the extreme field lines having the same connectivity as the oscillating (highlighted with red) field line.

(A color version of this figure is available in the online journal.)

of the AR. This good match confirms that a potential field extrapolation is a reasonable representation of the large-scale magnetic structure of this AR at the time of the observations. The bottom panels of Figure 12 show two further views of the AR. The field line showing the best correspondence with the vertically oscillating loop is highlighted with a thick red line. The loop is clearly not vertical and at first sight seems not to be central either. However, we note that the closed field lines are clustered in several groups connecting to different photospheric patches of field. In particular, the negative pole in panels (a) and (b) of Figure 12 is divided into two main parts in addition to various smaller patches. As such we should consider the relative position of the loop in the particular group of field lines having the same connectivity. We therefore determined the two extreme field lines having the same connectivity as the red field line and highlighted them with purple and blue thick lines. The extreme field lines are determined by checking the connectivity for the field lines originating from all the pixels and finding the most extreme position of such field lines, i.e., the field lines with the smallest and largest inclination angles. The observed

loop is clearly central within the cluster of loops of the same connectivity.

5. SUMMARY AND CONCLUSIONS

We present three-dimensional oscillations of dipolar AR loops with gravitationally stratified density. We study the effect on kink oscillations of the location within the AR of the oscillating loop and the exciting pulse. We find that pure vertical oscillations can be excited in central (symmetric) loops in a dipolar AR (which is considered as a set of loops connecting two spots of opposite polarity) if the pulse acts from roughly below the loop. If the pulse is moved further away from the central loop, the amplitude of the horizontal mode increases compared to the vertical one and a combination of vertical and horizontal modes is excited. Consequently, in central AR loops vertical oscillations are almost always excited—either as a pure mode or as a combination of modes with the horizontal oscillation. Most loops, however, are non-symmetric within the AR (*inclined* in the case of the geometry considered here). The *inclined* loops studied by us oscillate in a dominantly horizontal mode. Two extremely different locations of the exciter both lead to a nearly pure horizontal oscillation in loops with different (non-zero) inclination angles. These results do not depend on the geometry of the loop (*open* versus *closed* geometry). The observational studies of Nakariakov et al. (1999), Aschwanden et al. (1999), Schrijver et al. (2002), Verwichte et al. (2004), and Wang et al. (2008) imply that most of the oscillating loops display the horizontal mode. As most of the observed loops are located non-symmetrically among the field lines connecting two compact regions of concentrated magnetic flux, our model provides an explanation why most of the observed kink oscillations are horizontally polarized.

We compare our results, obtained for dipolar loops, with an observational example of vertical mode oscillation. The comparison indicates that for a loop to display vertical kink oscillations the symmetric location of the loop within the field lines, rather than its vertical orientation is necessary. Given the low plasma β in the corona this makes sense. Thus, in the observed case, the vertical mode is excited in the central loop within the bundle of field lines connecting two compact regions (sunspots) of opposite magnetic polarity by the perturbation from below the loop.

We find that, in contrast to the findings of Pascoe et al. (2009), a slow wave is excited in the loop even if the attack angle is small (perturbation located in front of the loop's apex). The difference between these results might be caused by the fact that a dipolar AR consists of loops for which the inclination angle varies, while in the arcade considered by Pascoe et al. (2009) the loop system consisted of an arcade of nearly identical loops. Therefore in a dipolar AR the pulse launched in the horizontal component of velocity will reach the loop as a combination of different components of velocity and will excite both kink and slow waves.

M.S.'s and L.O.'s work was financially supported by the NASA SEC Theory program and NASA grants NNG06GI55G and NNX09AG10G. S.K.S.'s work has been partially supported by the WCU grant No. R31-10016 funded by the Korean Ministry of Education, Science and Technology. The three-dimensional MHD computations were performed at NASA's Advanced Supercomputing (NAS) center.

REFERENCES

Aschwanden, M. J., De Pontieu, B., Schrijver, C. J., & Title, A. M. 2002, Sol. Phys., 206, 99
Aschwanden, M., Fletcher, L., Schrijver, C., & Alexander, D. 1999, ApJ, 520, 880
Aschwanden, M., Nakariakov, V., & Melnikov, V. 2004, ApJ, 600, 458
Berghmans, D., & Clette, F. 1999, Solar Phys., 186, 207
Brady, C. S., & Arber, T. D. 2005, A&A, 438, 733
Brady, C. S., Verwichte, E., & Arber, T. D. 2006, A&A, 449, 389
Cuperman, S., Ofman, L., & Semel, M. 1990, A&A, 227, 583
De Moortel, I., Ireland, J., Walsh, R. W., & Hood, A. W. 2002, Sol. Phys., 209, 61
Díaz, A. J. 2006, A&A, 456, 737
Díaz, A. J., Zaqarashvili, T., & Roberts, B. 2006, A&A, 455, 709
Gruszecki, M., Murawski, K., Selwa, M., & Ofman, L. 2006, A&A, 460, 887
Kliem, B., Dammasch, I. E., Curdt, W., & Wilhelm, K. 2002, ApJ, 568, L61
McLaughlin, J., & Ofman, L. 2008, ApJ, 682, 1338
Nakariakov, V. M., Aschwanden, M. J., & Van Doorsselaere, T. 2009, A&A, 502, 661
Nakariakov, V. M., Melnikov, V. F., & Reznikova, V. E. 2003, A&A, 412, 7
Nakariakov, V. M., Ofman, L., Deluca, E. E., Roberts, B., & Davila, J. M. 1999, Science, 285, 862
Nakariakov, V. M., & Verwichte, E. 2005, Coronal Waves and Oscillations, Living Rev. Solar Phys., 2, 3, (http://www.livingreviews.org/lrsp-2005-3)
Ofman, L. 2007, ApJ, 655, 1134
Ofman, L. 2009, Space Sci. Rev., 149, 153
Ofman, L., & Thompson, B. 2002, ApJ, 574, 440
Pascoe, D. J., De Moortel, I., & McLaughlin, J. A. 2009, A&A, 505, 319
Robbrecht, E., Berghmans, D., & Poedts, S. 1999, in Plasma Dynamics and Diagnostics in the Solar Transition Region and Corona, ed. J.-C. Vial & B. Kaldeich-Schümann (ESA SP-446; Noordwijk: ESA), 575
Ruderman, M. S., & Erdélyi, R. 2009, Space Sci. Rev., 149, 199
Schrijver, C. J., Aschwanden, M. J., & Title, A. M. 2002, Sol. Phys., 206, 69
Schrijver, C. J., & Brown, D. S. 2000, ApJ, 537, L69
Selwa, M., Murawski, K., Solanki, S. K., & Wang, T. J. 2007, A&A, 462, 1127
Selwa, M., Murawski, K., Solanki, S. K., Wang, T. J., & Shumlak, U. 2006, A&A, 454, 653
Selwa, M., Murawski, K., Solanki, S. K., Wang, T. J., & Tóth, G. 2005, A&A, 440, 385
Selwa, M., & Ofman, L. 2009, Ann. Geophys., 27, 3899
Selwa, M., & Ofman, L. 2010, ApJ, 714, 170
Selwa, M., Ofman, L., & Solanki, S. K. 2011, ApJ, 726, 42
Van Doorsselaere, T., Debosscher, A., Andries, J., & Poedts, S. 2004, A&A, 424, 1065
Van Doorsselaere, T., Verwichte, E., & Terradas, J. 2009, Space Sci. Rev., 149, 299
Verwichte, E., Foullon, C., & Nakariakov, V. 2006a, A&A, 446, 1139
Verwichte, E., Foullon, C., & Nakariakov, V. 2006b, A&A, 449, 769
Verwichte, E., Foullon, C., & Nakariakov, V. 2006c, A&A, 452, 615
Verwichte, E., Nakariakov, V. M., Ofman, L., & Deluca, E. E. 2004, Sol. Phys., 223, 77
Wang, T. J., Innes, D. E., & Qiu, J. 2007, ApJ, 656, 598
Wang, T. J., & Solanki, S. K. 2004, A&A, 421, L33
Wang, T. J., Solanki, S. K., Curdt, W., Innes, D. E., & Dammash, I. E. 2002, ApJ, 574, L101
Wang, T. J., Solanki, S. K., Curdt, W., Innes, D. E., Dammash, I. E., & Kliem, B. 2003, A&A, 406, 1105
Wang, T. J., Solanki, S. K., Innes, D. E., & Curdt, W. 2005, A&A, 435, 753
Wang, T. J., Solanki, S. K., & Selwa, M. 2008, A&A, 489, 1307